



## Muons and Neutrinos 2007

THOMAS GAISSER

Bartol Research Institute, Department of Physics and Astronomy, University of Delaware, Newark, DE 19716, U.S.A.

gaisser@bartol.udel.edu

**Abstract:** This paper is the written version of the rapporteur talk on Section HE-2, *muons and neutrinos*, presented at the 30th International Cosmic Ray Conference, Mérida, Yucatan, July 11, 2007. Topics include atmospheric muons and neutrinos, solar neutrinos and astrophysical neutrinos as well as calculations and instrumentation related to these topics.

## Introduction

There were 5 sections of contributed papers on muons and neutrinos with a total of 107 papers distributed as shown in Table 1. The most active category is HE 2.3, *astrophysical neutrinos*. Particularly in this area, there were also many papers presented in OG 2.5 sessions, on *high-energy astrophysical neutrinos*. I include discussion of these topics to the extent necessary to present a coherent overview of the field as of mid-year 2007.

Table 1: Papers on muons and neutrinos

Session	Topic	#
HE 2.1	Muon experiments	17
HE 2.2	Observations of solar & atmospheric $\nu$	16
HE 2.3	Observations of astrophysical $\nu$	37
HE 2.4	Theory and simulations	19
HE 2.5	New experiments & instrumentation	18

## Atmospheric muons

Muons are the gold standard of cosmic-ray physics because they are well-measured and their physical origin in the atmospheric cosmic-ray cascade is well-understood. A summary of measurements

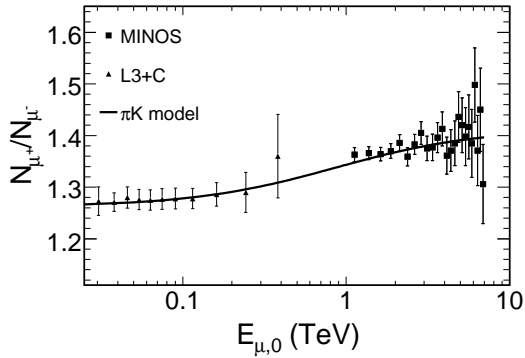


Figure 1: Muon charge-ratio from Ref. [4]. The line “ $\pi K$ ” model corresponds to a fit to the ratio of  $\mu^+/\mu^-$  from Eq. 1.

is included in this conference in Ref. [1]. Muons are penetrating and relatively abundant in all terrestrial particle detectors. They are therefore a potential source of background, and at the same time they are useful for detector calibration. One use of cosmic-ray muons is as a survey tool, sometimes called muon tomography. A classic example is the survey of the Second Pyramid of Giza and the search for hidden chambers [2]. The status of a similar investigation of the Pyramid of the Sun at Teotihuacan was presented at this conference [3]. The detector is integrated and ready for installation during 2008 in the tunnel that goes under the pyramid.

An important new result presented at this conference is the measurement of the muon charge ratio in the far detector of MINOS [4, 6, 5]. Muons that reach the detector at its depth of 2070 meters-water-equivalent (m.w.e.) have energies at the surface in the range of 1-7 TeV, depending on zenith angle. Fig. 1 from Ref. [4] shows muon charge ratio increasing in the energy range from  $E_\mu < 100$  GeV to  $E_\mu > 1$  TeV. The potential significance of this result can be understood from the energy-dependence of Eq. 1.

An approximate, first-order expression for the muon intensity for  $E_\mu > 100$  GeV is [7]

$$\phi_{\mu^\pm} = \frac{\phi_0(E_\mu)}{1 - Z_{N\pi}} \times \left\{ \frac{A_{\pi\mu} Z_{N\pi^\pm}}{1 + B_{\pi\mu} E_\mu \cos \theta / \epsilon_\pi} + \frac{A_{K\mu} Z_{NK^\pm}}{1 + B_{K\mu} E_\mu \cos \theta / \epsilon_K} \right\}, \quad (1)$$

where  $Z_{N\pi}$  and  $Z_{NK}$  are spectrum weighted moments for production of pions and kaons,  $\phi(E) \equiv E \, dN/dE$  and  $\phi_0(E_\mu)$  is the intensity of primary cosmic-ray nucleons evaluated at the energy of the muon. The kinematic factors are  $A_{\pi\mu} \approx 0.67$ ,  $A_{K\mu} \approx 0.25$  (including the branching ratio for  $K \rightarrow \mu\nu$ ),  $B_{\pi\mu} \approx 1.07$  and  $B_{K\mu} \approx 1.13$ .

Zatsepin and Kuz'min pointed out long ago [8] the potential of a measurement of the atmospheric muon flux as a function of zenith angle for measuring the relative importance of kaon to pion production in hadronic interactions. The angular dependence arises from the denominators of the two terms in Eq. 1 and the numerical values of the critical energy parameters,  $\epsilon_\pi \approx 115$  GeV and  $\epsilon_K \approx 850$  GeV. In the TeV range, the kaon contribution is relatively more important near the vertical than at large angle. Thus the angular dependence of the muon flux is sensitive to the ratio  $Z_{NK}/Z_{N\pi}$ . The angular dependence of the muon charge ratio provides information on the relative importance of kaons and pions separated by charge. By fitting the data of Fig. 1 to the charge ratio calculated from Eq. 1, the MINOS group find

$$\frac{Z_{N\pi^+}}{Z_{N\pi^+} + Z_{N\pi^-}} = 0.55 \quad (2)$$

and

$$\frac{Z_{NK^+}}{Z_{NK^+} + Z_{NK^-}} = 0.67. \quad (3)$$

The ratio  $(Z_{NK^+} + Z_{NK^-}) / (Z_{N\pi^+} + Z_{N\pi^-})$  has been kept fixed at its standard value. The fit uses the data of Refs [4, 10], which have data binned both in  $E_\mu$  and  $\cos \theta$ . The preliminary measurement of the charge ratio in the shallow MINOS near detector [9] (not shown) is consistent with the L3+C data. The large value of the  $K^+/K^-$  ratio reflects the importance of forward associated production ( $p \rightarrow \Lambda \, K^+$ ) which is amplified in the spectrum-weighted moment by the steep primary cosmic-ray spectrum because the  $K^+$  carries on average a significant fraction of the beam energy.

Two other papers from MINOS are noteworthy as examples of the use of cosmic-ray muons for calibrating deep detectors. More than 20 million muons were measured (after cuts) in the MINOS far detector over a three-year period from August 2003 to August 2006. One analysis uses the shadow of the moon to determine the angular resolution and absolute pointing of the far detector [11]. Both the resolution and the absolute pointing are  $0.3^\circ \pm 0.05^\circ$ . The moon's shadow is seen at the level of  $4 \, \sigma$ . The shadow of the sun is also seen, but at a somewhat lower significance, in part because of bending of the parent cosmic rays in the solar magnetic field.

Another paper [12] presents the analysis of seasonal variations of the underground muon rate observed in the MINOS far detector. The observed rate of muons is correlated with temperature by

$$\frac{\Delta R_\mu}{\langle R_\mu \rangle} = \alpha^T \times \frac{\Delta T_{\text{eff}}}{\langle T_{\text{eff}} \rangle}, \quad (4)$$

where  $T_{\text{eff}}$  is an average of the temperature weighted by the probability of meson production, which peaks at altitudes around 15 km for trajectories near the vertical. This correlation is explained in the classic paper of Barrett et al. [13] as a consequence expansion of the atmosphere when temperature increases. The correlation is large for muons with  $E_\mu \gg \epsilon_\pi$  where there is a competition between decay and re-interaction of the parent pion. At lower energies, most pions decay before interacting for any temperature. The observed rate,  $R_\mu$ , shows a seasonal variation of  $\approx \pm 2\%$  and corresponds to a value of  $\alpha_T = 0.87 \pm 0.03$ , consis-

tent with earlier measurements by MACRO [14] and AMANDA [15].

## Atmospheric neutrinos

Similar equations to Eq. 1 describe the flux of atmospheric neutrinos at high energy. However, the kinematic factors differ in an important way. Because its mass is close to that of the pion, the muon carries most of the energy in the  $\pi \rightarrow \mu\nu$  decay. The decay  $K \rightarrow \mu\nu$  is more nearly symmetric. As a result, while the kinematic parameters for  $K \rightarrow \nu$  are nearly equal to those for  $K \rightarrow \mu$ , they are quite different for pions. In particular,  $A_{\pi\nu} \approx 0.088$  as compared to  $A_{\pi\mu} \approx 0.67$ . As a consequence, the dominant contribution to neutrinos with  $E_\nu > 100$  GeV is from kaons, and the effect of the large charge ratio for kaons has a strong influence on the atmospheric neutrino spectrum at high energy. The tendency is to harden the TeV neutrino spectrum and to increase the ratio  $\nu_\mu/\bar{\nu}_\mu$ .

It is now widely accepted that the deficit of atmospheric muon-neutrinos with its pathlength and energy dependence is the result of neutrino oscillations. At this conference, there were only two papers concerning calculation of the flux of atmospheric neutrinos. Reference [16] estimates and tracks the various sources of uncertainty through the calculation in order to evaluate the systematic uncertainty in the flux of atmospheric neutrinos as a function of neutrino energy. The contribution of Honda et al. [17], focuses on evaluation of relatively small effects such as variation with solar cycle and the effect mountainous overburden above the detector. Ref. [17] is based on a revised calculation [18] that uses a new model of meson production in hadronic interactions [19] based on comparison to measurements of atmospheric muons. The new Honda et al. neutrino flux is now closer to the Bartol neutrino flux [16, 20] at high energy than the earlier calculation [21]. In both models now, the ratio  $Z_{pK^+}/Z_{pK^-}$  is large, consistent with the interpretation of the increase in the  $\mu^+/\mu^-$  ratio in the TeV region discussed above. The corresponding effect here is that the ratio  $\nu/\bar{\nu}$  is large ( $\sim 1.7$ ) in the TeV range). Moreover, the TeV neutrino flux is relatively high because of the importance of forward associated production on the

steep cosmic-ray spectrum. (An independent confirmation of the relatively high atmospheric neutrino flux in the TeV range comes from the work of Ref. [22], which assumes the best fit oscillation parameters and unfolds the atmospheric neutrino spectrum from the Super-K measurements.) The implications for atmospheric neutrinos of the MINOS measurement of the muon charge ratio have yet to be investigated in detail, however. It should be possible to use the MINOS data to reduce the uncertainty in existing calculations of the flux of atmospheric neutrinos in the TeV region and above.

## Neutrino oscillations

Super-Kamiokande has been restored to its full complement of over 11,000 50 cm photomultipliers plus an outer veto detector and has been operating since July 12, 2006 as Super-Kamiokande-III. Reference [26] reviews the history of Super-K, which began operation in April 1996 and announced the discovery of oscillations of atmospheric neutrinos in 1998 [27]. The phase of operation up to the accident in November, 2001 is SK-I. The detector was repaired and operated with some 5000 PMTs redistributed to provide uniform but sparser coverage. SK-II ran for three years, starting October, 2002. Preliminary results of SK-III are in agreement with SK-I and SK-II.

A series of Super-K papers at this conference presented preliminary results of the combined analysis of SK-I (1489 days) and SK-II (804 days). Atmospheric neutrino results, for example, were presented [29] in the same format as the main SK-I paper [28]. The plots of zenith angle show a ratio of  $(\nu_e + \bar{\nu}_e)/(\nu_\mu + \bar{\nu}_\mu)$  that is significantly higher than expectation for sub-GeV neutrinos from all directions, and a deficit of multi-GeV neutrinos from below ( $\sim 10,000$  km) but consistent with expectation from above ( $\sim 15$  km). The angular distribution of the electron neutrinos has the expected (no oscillation) shape. The results are fully consistent with two-flavor  $\nu_\mu \leftrightarrow \nu_\tau$  oscillations with transition probability

$$P_{\nu_\mu \leftrightarrow \nu_\tau} = \sin^2(2\theta_{23}) \times \sin^2 \left[ 1.27 \frac{\delta m^2 (\text{eV}^2) L_{\text{km}}}{E_{\text{GeV}}} \right]. \quad (5)$$

The dip at the first oscillation minimum in  $L/E$  is seen [30] for atmospheric neutrinos [31], and there is no evidence yet for three-flavor effects such as non-zero  $\theta_{13}$ .

The MINOS group also presented their results for neutrino oscillations using the NuMI muon-neutrino beam from Fermilab [32]. The results, already published, [33] show a deficit of muon neutrinos in the far detector relative to the near detector over a distance of 735 km that is consistent with the results of the Super-K atmospheric neutrino result. The MINOS far detector can also measure  $\nu_\mu$ -induced upward muons with charge separation. Although statistics are limited, they see a deficit of lower-energy neutrino-induced muons consistent with the Super-K oscillation parameters [34]. An interesting feature of neutrino-induced muons in a magnetized detector is that the charge ratio can be measured. The charge ratio is opposite to that for atmospheric muons because positive mesons ( $\pi^+$  and  $K^+$ ) decay to  $\mu^+$  and  $\nu_\mu$  (which produce  $\mu^-$ ), while negative mesons give  $\bar{\nu}_\mu$  (which produce  $\mu^+$ ).

During the time that Super-K II operated with half the density of PMTs as compared to Super-K I, new reconstruction algorithms were developed that allowed sensitivity similar to that of the original detector. Now that the detector has been restored to its full complement of PMTs, the better algorithms make it possible to lower the energy threshold [35]. Super-K III currently is operating with 100 per cent trigger efficiency down to 5 MeV, which is in the transition region from matter dominated to vacuum oscillations for solar neutrinos.

### Astrophysical neutrinos (low energy)

Neutrinos from SN1987A in the Large Magellanic Cloud are so far the only neutrinos detected [36, 37] from outside the solar system. A network of several deep detectors continues to monitor the sky for bursts of neutrinos from nearby stellar collapses. New upper limits on the rate of stellar collapse in the Milky Way Galaxy based on non-observation of neutrino bursts are summarized in Table 5.

It is also possible to search for a diffuse flux of relic neutrinos from past supernova explosions. The

Table 2: Limits on supernova rates in the Milky Way Galaxy (events per year at 90% c.l.). The Super-K limit includes SMC and LMC.

Experiment	Exposure	Limit
S-K [44]	2589 d	0.30
LVD [45]	4919 d	0.17
Baksan [46]	22 yr	0.10

spectrum of these relic neutrinos peaks at a few MeV and falls quickly with increasing energy [38]. The process

$$\bar{\nu}_e + p \rightarrow n + e^+ \quad (6)$$

with its relatively large cross section is the preferred channel for this search [39]. The convolution of the cross section, which increases with energy, and the spectrum of relic neutrinos may be above the expected background from atmospheric  $\bar{n}$  in a window of energy from  $\sim 10$  to 20 MeV [40]. Current limits from Super-K [41] are close to the signals expected from various models, as shown in Ref. [43] at this conference. The possibility [40] of adding Gadolinium to tag recoil nucleons from the process of Eq. 6 was mentioned at this conference in Ref. [35]. A test of this method with a 2.4 liter container of  $\text{GdCl}_3$  and a radioactive source is described in Ref. [42].

### Astrophysical neutrinos (high energy)

The most promising channel to use in the search for astrophysical neutrinos of high energy ( $> \text{TeV}$ ) is neutrino-induced muons because the effective volume of the detector is amplified by the muon range. The average energy loss rate of a muon per  $X(\text{g/cm}^2)$  of material traversed is

$$\frac{dE}{dX} = -a - bE, \quad (7)$$

where  $\epsilon = a/b \sim 0.5 \text{ TeV}$  is the characteristic energy above which stochastic losses (bremsstrahlung and nuclear interactions) begin to dominate the energy loss. The corresponding average muon range is

$$X \approx \frac{1}{b} \times \ln \left( \frac{E_{\mu,0} + \epsilon}{E_{\mu,\min} + \epsilon} \right), \quad (8)$$

where  $E_{\mu,0}$  is the muon energy at production and  $E_{\mu,\min}$  is the threshold energy of the detector for muons. The muon range can be several kilometers or more in water or ice.

When only the muon is detected, however, there is only an average relation between the visible energy of the muon and that of the neutrino that produced it. The fraction of the neutrino energy carried by the muon varies from event to event, and the track is only partially contained. Moreover, for  $E_\mu \gg \epsilon$  there are large fluctuations in the amount of visible energy deposited as the high-energy muon passes through the detector [23]. Nevertheless, because the relation between energy deposition of the muon as it passes through the detector and its total energy is well understood (as well as the relation between the energy of the muon and that of the neutrino that produced it), it is straightforward to derive the parent neutrino spectrum from a measurement of neutrino-induced muons given sufficient statistics. From a Monte Carlo simulation of the detector response one has to identify a set of measurable quantities that depend on energy deposition in the detector. An unfolding procedure can then be used to reconstruct the parent spectrum. The error analysis must account for the large fluctuations from event to event. A prescription using the photon density along the muon track as the energy-dependent observable for reconstruction and unfolding the atmospheric neutrino spectrum in IceCube is given in Ref. [24]. This is a natural choice given the physics of muon energy loss described by Eq. 7.

The high-energy tail of the spectrum of atmospheric neutrinos constitutes the background for searches for neutrinos from astrophysical sources. Atmospheric neutrinos also serve as the calibration beam. Atmospheric neutrinos are sufficiently well-understood in the multi-TeV range so that successful reconstruction of their spectrum can be considered as a prerequisite to any search for astrophysical neutrinos. As an example, Fig. 2 shows the atmospheric neutrino spectrum derived by an unfolding procedure from AMANDA data taken from 2000-2003 [25].

An important remaining uncertainty in the atmospheric neutrino flux at high energy is the level of the contribution from prompt neutrinos. These are neutrinos from the decay of charmed hadrons

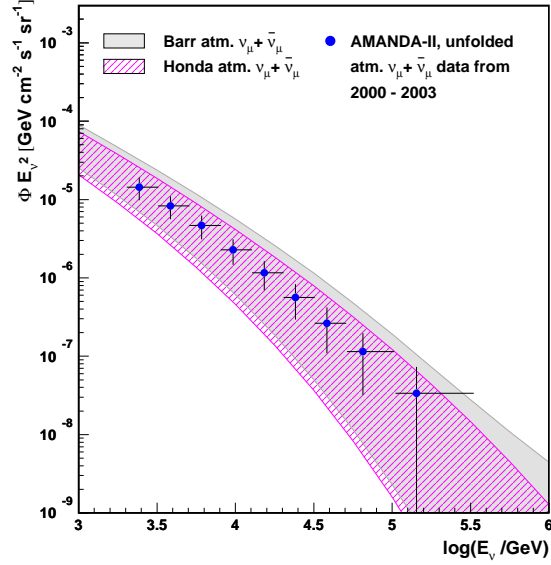


Figure 2: Unfolded spectrum of atmospheric neutrinos by AMANDA-II [25] compared to calculations of Refs. [20, 21].

which have a harder spectrum than neutrinos from decay of pions and kaons, which are suppressed at high energy because the parent mesons tend to interact rather than decay. The prompt contribution to the atmospheric lepton flux can be represented by adding a third term to the right hand side of Eq. 1 of the form

$$\frac{A_C Z_{N,C}}{1 + B_C E \cos \theta / \epsilon_C},$$

where the subscript "C" represents a charmed hadron, E is the lepton energy ( $\mu$ ,  $e$ ,  $\nu_\mu$  or  $\nu_e$ ) and  $\epsilon_C \sim 2 - 9 \times 10^7$  for a range of charmed hadrons with significant leptonic branching ratios [49]. For muon neutrinos with  $E_\nu > \epsilon_K = 850$  GeV the spectrum gradually steepens from  $E^{-2.7}$  to  $E^{-3.7}$  while the spectrum of prompt neutrinos continues to reflect the primary cosmic-ray spectrum until  $E_\nu = \epsilon_C \sim 3 \times 10^7$  GeV. The crossover energy depends on the amount of charm production in hadronic interactions at high energy ( $Z_{N,C}$ ), which is highly uncertain, particularly in the fragmentation region. For a model with a significant contribution of intrinsic charm [50] the neutrinos from charm decay become the dominant component of atmospheric  $\nu_\mu$  for  $E_\nu > 100$  TeV [51]. For the

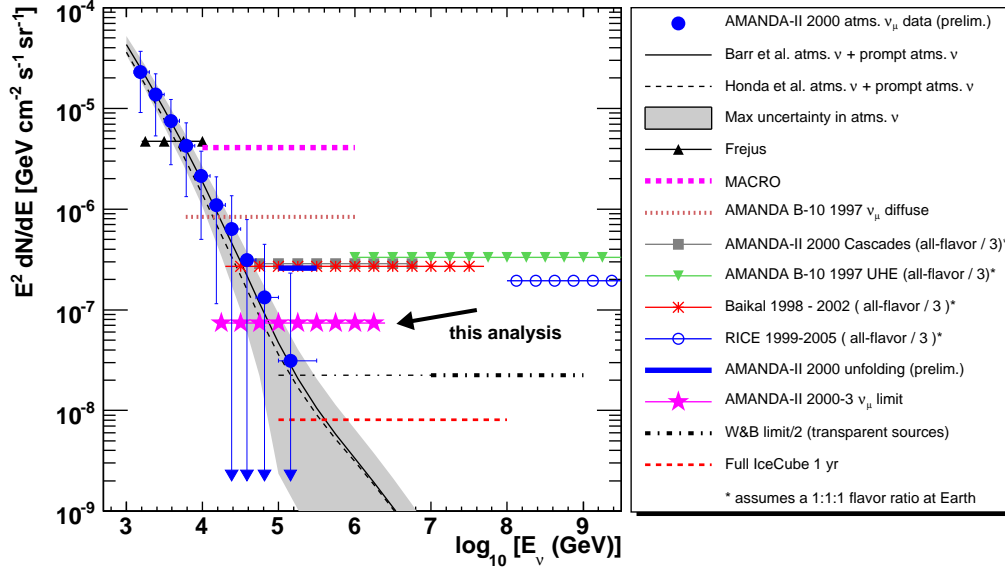


Figure 3: Limit on the diffuse flux of astrophysical neutrinos from AMANDA-II [48].

much steeper spectrum of  $\nu_e$  the crossover of the charm component is around 3 TeV.

**Diffuse search.** High-energy astrophysical neutrinos are expected to be produced by interaction of high-energy accelerated particles with gas or electromagnetic radiation in or near the sources. Generally the particle beams, and hence the produced neutrinos, are expected to have a harder energy spectrum than the background atmospheric neutrinos. A standard benchmark for high-energy neutrinos of extra-galactic origin is the Waxman-Bahcall limit [47], which assumes an  $E^{-2}$  differential spectrum. The normalization of the Waxman-Bahcall limit for  $\nu_\mu + \bar{\nu}_\mu$  at Earth after accounting for oscillations is  $E^2 dN_\nu/dE < 2.2 \times 10^{-8} \text{ GeV cm}^{-2} \text{ s}^{-1} \text{ sr}^{-1}$ . To exceed this level would require the existence of cosmic accelerators opaque to the particles they accelerate. The limit might also be relaxed to some extent at lower energy in the case of steeper source spectra.

Figure 3 shows current limits on a diffuse flux of neutrinos with an  $E^{-2}$  differential energy spectrum from AMANDA. The figure illustrates several points. The search labeled "this analysis" looks for neutrino-induced muons generated in the

ice and rock below the detector. This is the energy region and the signature for which existing large detectors in deep water or ice are optimized. Such a search is limited to neutrinos with  $E_\nu < 1 \text{ PeV}$  because the Earth absorbs neutrinos with higher energy.

In the PeV energy region and above a diffuse signal would be dominated by events near the horizon, where the target length is maximized without absorbing the neutrinos. Here one is generally looking for events characterized by large and concentrated depositions of energy, either radiating  $\nu_\mu$ -induced muons or cascades from interactions of  $\nu_e$  or  $\nu_\tau$  in or near the detector. Fig. 3 includes the limit from the Baikal experiment in this energy range. The "all-flavor" limit is divided by three on the plot to make it comparable with the limits on  $\nu_\mu$  alone. A preliminary value of  $2.4 \times 10^{-7} \text{ GeV cm}^{-2} \text{ s}^{-1} \text{ sr}^{-1}$  was presented at this conference for the upper limit of all neutrino flavors from AMANDA in the "UHE" energy range  $10^5 < E_\nu < 10^9 \text{ GeV}$  [52]. This is approximately a factor of three below the Baikal limit and only slightly higher than the limit from up-

ward muons [48] in the energy range around 1 PeV where both limits apply.

The "diffuse" limit on any particular model spectrum is obtained by convolving the spectrum with the detector response. In the case of the diffuse limits for an  $E^{-2}$  spectrum, the plotted limit is a horizontal line on a plot of  $E^2 dN/dE$  extending over the energy region that gives 90% of the signal. In general, a separate limit must be calculated for each assumed model spectrum. Ref. [52] gives a useful table of models and sensitivities that specifies which models are inconsistent at 90% confidence level with the present AMANDA UHE diffuse limit. Several early models of neutrino production in AGN are ruled out, including, for example Ref. [53], while others (e.g. [54, 55]) are still viable.

In the case of searches for UHE neutrinos with optical detectors the signal would be characterized by a large amount of light in the detector. Since the events will be from above and from the sides, an important background is from bundles of muons generated by high-energy cosmic rays cascades in the atmosphere. Showing that this physical background is well-understood (for example by comparing simulations with data at various cut levels) is needed to demonstrate understanding of the detector response. A feature used to discriminate between signal and background in Ref. [52] is the number of optical modules with multiple hits versus single hits. Muon bundles from cosmic-ray cascades tend to produce less light per particle, and the source of the light is somewhat diffuse as compared to the intense and concentrated burst of light from a single particle with energy in the PeV range or higher. The signal would produce more multiple hits.

**Point sources.** Particularly luminous and/or nearby sources of neutrinos should eventually emerge above the diffuse atmospheric background. Likely candidates are the subset of gamma-ray sources in which the gamma-rays are hadronic in origin, from decay of neutral pions produced in interactions of accelerated protons and nuclei in or near the sources. The kinematic relation between  $\pi^0 \rightarrow \gamma\gamma$  and  $\pi^+ \rightarrow \mu^+ \nu_\mu$  provides a close connection between neutrinos and gamma-rays if the photons are not significantly absorbed in the sources. Examples of potential sources

are Active Galactic Nuclei (AGNs), Gamma-ray Bursts (GRBs) and supernova remnants and active compact objects in our galaxy. Since it is still not known which gamma-ray sources are hadronic, identification of neutrinos from sources of gamma rays (and/or electromagnetic radiation in other wavelengths) is the central goal of high-energy neutrino astronomy.

As an example, it is interesting to consider likely sources of high-energy neutrinos in our local galaxy. In the Northern hemisphere, visible from Antarctica, the Cygnus region is of particular interest [56]. A systematic survey of the sensitivity of a future kilometer-cube neutrino detector in the Mediterranean to potential galactic sources visible from the North was given in Ref. [57]. (A more detailed discussion of the analysis is given in Ref. [59].) Table 3 summarizes results for those H.E.S.S. sources with spectra for which a break energy (where the spectrum steepens) has been determined. The corresponding neutrino spectrum would steepen at a somewhat lower energy than the observed steepening of the gamma-ray spectrum and about a factor of 40 lower than the energy at which the parent proton spectrum steepens. Assumptions of the calculation are that the observed gamma-ray spectrum is entirely hadronic in origin, produced by interaction of an accelerated spectrum of protons with gas in or near the source and that there is no absorption of gamma-rays in the source. A ratio at production of  $\nu_e : \nu_\mu : \nu_\tau = 1 : 2 : 0$  is assumed with a flavor ratio at Earth of  $1 : 1 : 1$ . The neutrino effective area of a  $\text{km}^3$  detector in the Mediterranean for the  $\nu_\mu + \bar{\nu}_\mu$  channel is calculated in some detail to obtain the expected number of events for source ( $N_{\text{src}}$ ) and background ( $N_{\text{atm}}$ ) by convolution with the spectrum of the source and with the atmospheric neutrino spectrum. However, efficiencies for event selection and reconstruction are not accounted for.

The results summarized in Table 3 nicely illustrate some important features of point source searches with kilometer-scale neutrino telescopes. The second and third columns of the table give the diameter of each gamma-ray source and the fraction of the time it is below the horizon. Typically, the source sizes exceed the resolution of H.E.S.S. and are comparable to or larger than the resolution of the neutrino telescope. If the characteristic neu-

Source name	Dia(°)	Vis	$\epsilon_\nu$ (TeV)	$E_\nu > 1$ TeV		$E_\nu > 5$ TeV	
				$N_{\text{src}}$	$N_{\text{atm}}$	$N_{\text{src}}$	$N_{\text{atm}}$
A: RX J0852.0-4622	2.0	0.83	1.19	11	104	4.2	21
A: RX J1713.7-3946	1.3	0.74	1.25	11	41	4.6	8.2
B: LS 5039 (INFC)	0.1	0.57	1.01	0.5	2.5	0.2	0.5
C: HESS J1303-631	0.3	1.0	0.21	1.6	11	0.3	2.1
D: Vela X	0.8	0.81	0.84	16	23	10	4.6
D: HESSJ1825-137	0.5	0.57	4.24	8	9.3	3.7	1.8
D: Crab Nebula	<0.1	0.39	1.72	5.8	5.2	1.9	1.1

Table 3: TeV galactic  $\gamma$ -ray sources from the H.E.S.S. catalog [58] with corresponding neutrino rates calculated for 5 years operation of KM3NeT (1 km<sup>3</sup> instrumented volume) [59].

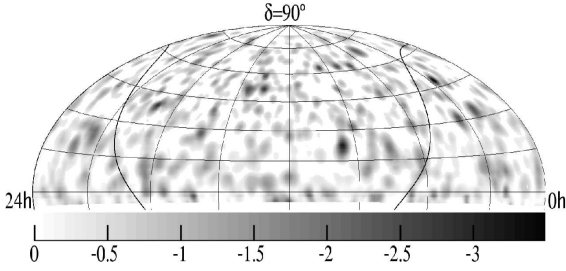


Figure 4: Preliminary sky map from Ref. [65] showing  $\log_{10}(p)$  for an unbinned point source search with AMANDA-II in 2005.

trino break energy is  $\geq 1$  TeV or higher, the signal to background ratio improves at higher energy, so the ability to measure a signal related to energy will be important. For neutrino sources that steepen in the TeV region, the signal/background improves by about a factor of two if the threshold can be raised from 1 to 5 TeV.

Expected rates are low, and signal/background is less than or comparable to unity depending on the size of the source. Techniques such as “source stacking” will therefore be important [60] to improve the significance. Similar conclusions about signal/background for such galactic source can be inferred from Ref. [61]. Hadronic models are disfavored for several of the types of sources listed. Prime candidates are A: shell-type SNRs and C: TeV  $\gamma$ -ray sources with no counterparts at other wavelengths. Pulsar wind nebulae (D) and binary systems (B) are more often explained with electromagnetic models, although hadronic models exist.

Traditional searches use a bin size around the source optimized for the source size and point spread function of the detector. In Ref. [57, 59], for example, the bin size is  $1.6 \times \sqrt{\sigma_{\text{PSF}}^2 + \sigma_{\text{src}}^2}$ . Unbinned likelihood procedures that improve sensitivity by using energy-dependence and time clustering (as well as direction) are discussed for ANTARES in Ref. [64], for AMANDA in Ref. [65] and for IceCube in Ref. [66]. Ref. [65] finds an improvement in sensitivity and discovery potential for AMANDA-II of 30% compared to the binned search. The ANTARES analysis [64] finds a greater improvement, up to a factor of two or more in some cases. Figure 4 illustrates the kind of confidence level map that results from an unbinned point source search.

**Variable sources.** For sources known to be variable in electromagnetic radiation, e.g. in X- or  $\gamma$ -radiation, the significance of a small number of neutrinos from the direction of that source could be greater if they occur at the same time as flares. Assessing the extra significance depends on the extent to which the pattern of flaring is understood. Ref. [62] proposes a method in which directions to sources such as specific AGN known to be variable in electromagnetic radiation are searched for time clusters of neutrinos on various time scales. When a significant fluctuation above background is found, a check is made to see if the source is in a high state in electromagnetic radiation at the same time. If not (or if the EM data are not available) a time-clustering algorithm is compared with a large set of Monte Carlo data samples from the selected set of sources to look for an excess over background. A similarly motivated approach [63]



looks for correlations on various time scales using known properties of the atmospheric neutrino background as part of the analysis.

The most straightforward approach to making use of variability in electromagnetic radiation from a potential neutrino source is to look for a correlation in the historical record between, for example, flares from blazars and times of neutrinos from the direction of the same sources. For coincidence with a gamma-ray telescope with nearly continuous coverage of a large part of the sky (e.g. Milagro or Tibet) this is a good approach [67]. For telescopes with a limited field of view, however (such as VERITAS, MAGIC, H.E.S.S.), the telescope will most likely be looking elsewhere when a neutrino signal occurs. If, as is likely, the neutrino events are not significantly above atmospheric background on their own, then no signal can be claimed. One way to address this asymmetry is to send an alert when a pre-specified condition is satisfied by the neutrino detector, which is continuously sensitive to the hemisphere below the detector. The gamma-ray telescope can then slew to the selected source and see if it is flaring. A test of such a neutrino-triggered "Target of Opportunity" (ToO) arrangement for a pre-selected set of sources was reported at this conference for AMANDA and MAGIC [68].

Another possibility is to define an alert as a group of neutrinos from the same direction within a pre-selected time window for any direction in the sky. Such a possibility is described in Ref. [69] where it is proposed to send an alert to optical cameras that can quickly point to the direction defined by the group of neutrinos. In this way it might be possible to discover the onset of an optical supernova or a GRB afterglow, which could elevate the significance of the neutrino observation from a chance coincidence of several atmospheric neutrinos to an identified astrophysical neutrino event.

**Gamma-ray bursts.** Neutrinos associated with gamma-ray bursts would have both a time tag and a location which would make the detection of even a small number of such neutrinos significant. Limits on neutrinos associated with gamma-ray bursts using AMANDA has been published recently [70, 71] and presented at this conference in Ref. [69]. The most sensitive search was in the  $\nu_\mu$ -induced muon channel [70], which used 400

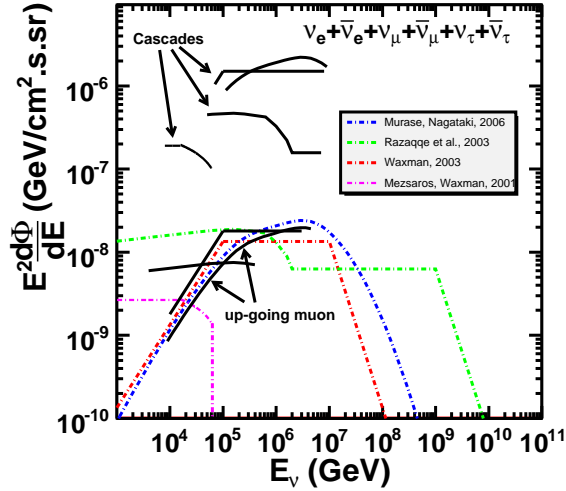


Figure 5: AMANDA limits on neutrinos from GRBs [69]. See text for discussion.

hundred bursts reported by BATSE and IPN3 between 1997 and 2003. No neutrinos were observed. Fig. 5 shows a comparison of limits with models. The three lines labeled "up-going muon" are limits for the models with the corresponding shapes. Thus the model of Ref. [72] is ruled out and the model of Ref. [73] is marginally incompatible with the limit. A  $3\sigma$  upper limit is set at 1.3 times the level predicted in the model of Waxman and Bahcall [74]. With IceCube the sensitivity for detection of neutrinos from GRBs will rapidly improve. IceCube is operating now with 22 strings and is expected to have 36 to 40 strings in operation by the time GLAST turns on in 2008. Assuming GLAST will observe some 200 GRBs per year over the whole sky, it is estimated [69] that observation of 70 bursts in the Northern hemisphere without associated neutrinos would be in conflict with the model of Ref. [74] at the  $\sigma$  level. This level of sensitivity should be possible with an exposure equivalent to one year of full IceCube.

## Cosmogenic neutrinos

There is now a growing consensus that the primary cosmic-ray spectrum becomes steeper above  $5 \times 10^{19}$  eV [75, 76, 77]. This is generally at-

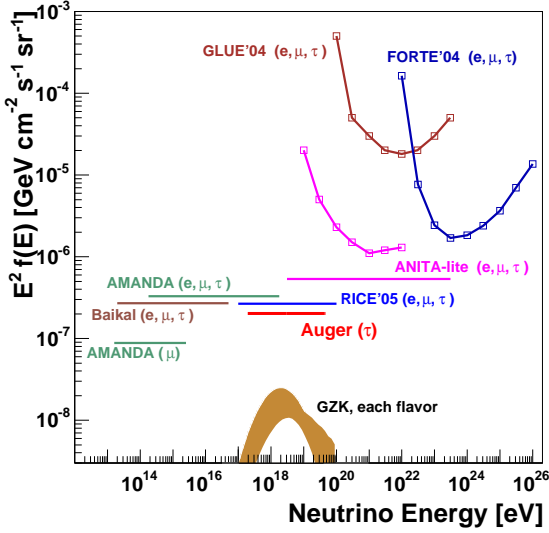


Figure 6: Figure from Ref. [80] showing upper limits from various experiments assuming  $\nu_e : \nu_\mu : \nu_\tau = 1 : 1 : 1$  at the detector. See text for a discussion of this figure.

tributed to the “GZK” effect [78, 79] of energy loss as particles interact with photons of the microwave background radiation during propagation from sources at cosmological distances. A lack of high energy particles could, however, also be due to a lack of sources capable of accelerating particles to energies of  $\sim 10^{20}$  eV. In any case, the number and spectrum of cosmogenic neutrinos is a key to the origin of the highest energy cosmic rays. Current measurements have not yet reached the sensitivity to detect cosmogenic neutrinos at the expected levels, as shown in Fig. 6 from Ref. [80].

Limits shown in Fig. 6 come from several types of detectors, which are sensitive to different ranges of energy and to different combinations of neutrino flavors. The Auger limit [80] is for the  $\nu_\tau$  channel for a period from January 2004 to December 2006 that corresponds to one year of operation of the full detector. The limit is shown for the energy region that would generate 90% of the signal for an  $E_\nu^{-2}$  differential spectrum, which overlaps well with the expected spectrum of cosmogenic neutrinos. A similar limit from Hi-Res [81] is essentially at the same level as the Auger limit. The air-shower

limits are based on searches for atypical horizontal showers as discussed in the next section.

For uniformity, limits from other experiments are shown in Fig. 6 assuming an equal mixture of the three neutrino flavors at Earth. Limits from the optical detectors, AMANDA [82, 48] and Baikal [83], are at lower energy. Limits from radio detectors include RICE [84] in the ice at the South Pole, ANITA-Lite [85], a balloon-borne radio detector looking for neutrinos interacting in the Antarctic ice sheet, and FORTE [86], searching for radio pulses from neutrino interactions in the Greenland ice mass. GLUE [87] looks for microwave signals of neutrino interactions in the Moon.

There are several calculations of the spectrum of cosmogenic neutrinos, which vary depending on assumptions about the spectrum and cosmological evolution of the cosmic-ray sources. The band shown in Fig. 6 is a range based on calculations by two groups [88, 89]. The calculation of Ref. [89] was discussed at this conference in [90] for two different models of the primary cosmic-ray composition. The result in the high-energy peak region ( $E_\nu \sim 10^{18}$  eV) is rather independent of the composition.

## Neutrino detectors and techniques

I conclude with a summary of the status of large neutrino detectors which have the primary aim of finding high energy ( $\geq \text{TeV}$ ) astrophysical neutrinos and identifying their sources. The discussion is organized by detection method. I do not include here the densely instrumented detectors such as MINOS and Super-K, which are aimed primarily at study of neutrino oscillations and (in the case of Super-K) low energy neutrinos and proton decay.

Because of oscillations, neutrinos from astrophysical sources are expected to consist of comparable numbers of all three neutrino flavors after propagation from distant sources. At production (whether in the atmosphere or in an astrophysical source) the production of  $\nu_\tau$  is strongly suppressed relative to  $\nu_\mu$  and  $\nu_e$ . For this reason, identification of  $\tau$ -neutrinos would be a signal of astrophysical neutrinos. The signature of a tau neutrino interaction

Detector	Number of OMs	enclosed vol. (m <sup>3</sup> )	depth (m.w.e.)	status
Baikal (NT200+)	230	$2 \times 10^6$	1100-1310	operating
AMANDA	677	$1.5 \times 10^7$	1350-1850	operating
ANTARES	900	$1 \times 10^7$	2050-2400	2007/2008
IceCube	1320	$1.8 \times 10^8$	1350-2250	2007
	4800	$10^9$	1350-2250	2011
KM3Net	~10,000	km <sup>3</sup>	2300-3300 (NEMO)	design study
		km <sup>3</sup>	3000-4000 (NESTOR)	
		km <sup>3</sup>	1400-2400 (ANTARES site)	

Table 4: Parameters of existing and proposed neutrino neutrino telescopes in water and ice.

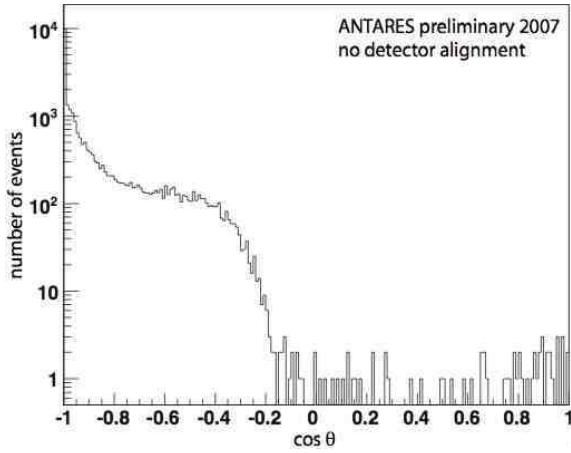


Figure 7: Figure from Ref. [91] showing angular distribution of reconstructed muons in 5 lines of ANTARES.

is expected to become recognizable at high energy where the produced  $\tau$ -lepton has a measurable decay length. The decay length is

$$\Gamma c\tau_\tau = 49 \text{ m} \times E_\nu (\text{PeV}). \quad (9)$$

Several papers at this conference focus on the phenomenology of  $\tau$ -neutrinos in the context of new experiments and the search for cosmogenic neutrinos.

**Optical detectors** Antares and IceCube build on the optical techniques of Baikal and AMANDA. Generally the water detectors have less scattering and therefore superior ability at track reconstruction and angular resolution than ice, while being subject to higher background noise rates due to radioactivity and bioluminescence. Fig. 7 from

Ref. [91] shows the preliminary angular distribution of reconstructed muon tracks. The isotropic distribution of muons induced by atmospheric neutrinos emerges from the background of downward muons already slightly above the horizon. This achievement reflects a combination of long scattering length and depth of the detector. At a depth of 2475 m, the intensity of penetrating atmospheric muons is almost an order of magnitude lower than at the top of IceCube (1450 m ice). At the time of the conference (July 2007), ANTARES had 5 lines operating in the ice. All 12 lines with a total 900 of optical modules are now in place and full operation of the detector is set to begin early in 2008. The status of various neutrino telescopes that use the optical Cherenkov technique is summarized in Table 4.

IceCube is currently operating with 22 strings and 1320 digital optical modules (DOMs) at depths of 1450 - 2450 m in the ice at the South Pole [92]. Results reported at this conference were from data taken with the 9 string configuration that operated during 2006. First observations of atmospheric neutrinos with IceCube-9 have been published [93]. The plan is to complete IceCube deployment over the next four austral summer seasons to its full size. The detector will operate and accumulate data while deployment is being completed. IceCube includes a surface component, IceTop [94], which ran with 16 stations during 2006 and is currently operating with 26 stations during 2007. Each station consists of two ice Cherenkov tanks, each of which is viewed by two DOMs. IceCube including IceTop constitutes a 3-dimensional air shower array that can study primary cosmic rays, including primary composition, from PeV to

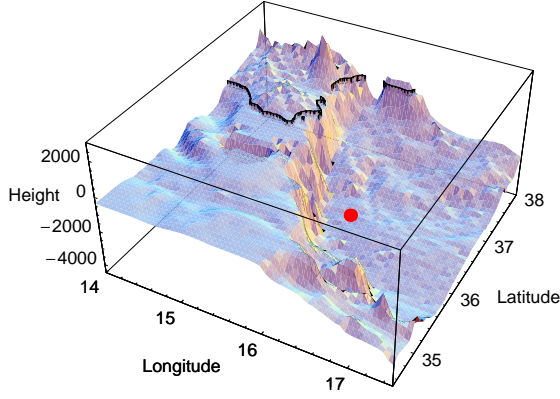


Figure 8: Surface map of the coast and sea floor of Eastern Sicily [103]. The line marks the shore-line, and the highest peak is Mt. Etna. The red dot indicates the proposed NEMO location.

EeV energy. AMANDA is now integrated into IceCube as a densely instrumented sub-array [95]. There is a common event builder so that every reconstructed event in AMANDA and/or IceCube contains the information about hits in the detectors of both components.

An important feature of the IceCube detection system is that waveforms of the signals are captured at 300 MHz. For events of high energy where many DOMs have multiple hits, use of full waveform information can improve the reconstruction. For example Ref. [96] finds  $\delta E/E \sim 0.34$  and  $\delta\psi \sim 0.6^\circ$  for thoroughgoing tracks with  $0.1 < E_\nu < 30$  PeV.

KM3Net is a consortium of the three Mediterranean experiments (ANTARES [91], NEMO [97] and NESTOR [98]) to design and build a kilometer-scale neutrino telescope in the Mediterranean. Several papers [99, 100] present studies of the configuration and sensitivity of a gigaton detector in the Mediterranean Sea. Of particular interest is the comparison of three sites [102, 103] for their sensitivities to neutrinos with energies  $E_\nu > 0.1$  EeV, the energy range of cosmogenic neutrinos. In this case, neutrino-induced  $\tau^\pm$  and  $\mu^\pm$  tracks passing through the detector are of comparable importance. The  $\nu_\tau$  channel is enhanced

by the possibility of interaction in nearby mountains from which the  $\tau$ -lepton can emerge and pass through the detector (see Fig. 8). The geometrical and kinematical situation are complicated by the competition among  $\nu_\tau$  interaction and regeneration in the Earth, by  $\tau$  energy loss and decay and by the configuration and response of the detector [101]. Accounting for these complications, the estimated rate is [102] 0.1 GZK neutrino interactions per  $\text{km}^3$  per year in a deep sea detector.

Because the Earth becomes opaque to neutrinos with  $E_\nu \sim \text{PeV}$  the angular distribution of neutrinos from below can in principle be used to measure the neutrino cross section by varying the path length through the Earth, corresponding to the nadir angle of the event. Given a sufficiently large flux of neutrinos it is conceivable to separate neutrino cross section from energy spectrum. Ref. [102] give examples of energy/angular dependence in the energy range 10 PeV to 1 EeV.

#### Giant air shower arrays as neutrino detectors.

Auger and other arrays can be used to look for horizontal air showers initiated near the detector by a neutrino interaction with  $E_\nu > 1$  EeV. Signature of a neutrino is a horizontal shower observed at the ground with a large electromagnetic component and time structure like that of a normal (nearly vertical) cosmic-ray shower. In contrast, the background of cosmic-ray induced horizontal showers consists mostly of muons with a sharp time structure of the shower front. The electromagnetic component of a horizontal air shower is absorbed far from the detector because of the large slant depth.

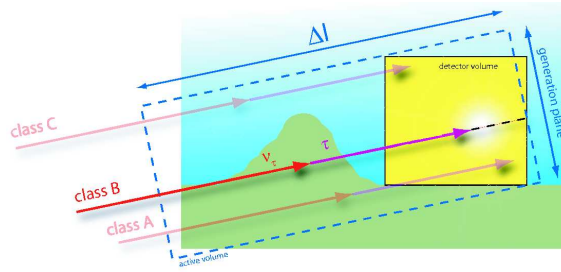


Figure 9: Diagram showing several trajectories of neutrino interactions that pass through the sensitive volume of Auger from below the horizon [104].

Horizontal showers from neutrinos are considered in two groups [101], those from above the horizon, which are dominated by charged current interactions of  $\nu_e$ , and those from below the horizon, which are mainly from  $\nu_\tau$  that interact in the surface of the Earth and produce a  $\tau$ -lepton that emerges from the ground and decays in the atmosphere in the field of view of the detector. The present limit from early operation of Auger is cited above (see Fig. 6). A detailed Monte Carlo simulation of Auger South to GZK neutrinos, accounting for the nearby Andes mountains, is given in Ref. [104] and illustrated in Fig. 9. The contribution of Earth-skimming  $\nu_\tau$  is enhanced by the presence of the Andes mountains. In Fig. 9 lines labeled A and B would be from decay of  $\tau$ -leptons, while C most often would be from the interaction of a  $\nu_e$ . Class C events can also arrive from above the horizon.

**Radio detection of neutrinos.** Given the low event rates expected from cosmogenic neutrinos in optical and air shower detectors, and in view of the importance of the measurement, efforts to find techniques that allow a much larger effective volume for detecting neutrinos in the EeV energy range are important. Using radio Cherenkov radiation from neutrino interactions in ice is one way to do this [105]. The Radio Antarctic Muon and Neutrino Detector (RAMAND) at the Vostok station was the first effort to investigate radio detection in ice [106]. In a paper at this conference [107] some of the originators of the radio technique report on a hybrid Monte Carlo code (SIMEX) that allows fast simulations of radio Cherenkov radiation from neutrino interactions [107]. The RICE detector at the South Pole [108] is still in operation using the same technique. Studies of radio detection in ice at the South Pole continued in the 2006-2007 season with the deployment of test receivers and transmitters by AURA [109].

Another approach is to use a balloon-borne detector looking down at the Antarctic ice sheet. Results from a prototype flight of ANITA are included in Fig. 6. The full ANITA detector flew over Antarctica for 35 days after launch on December 15, 2006 [110]. Results have not yet been reported. Before the flight, the detector was placed above a large block of ice illuminated by an intense, pulsed electron beam at SLAC [111]. Measurements of

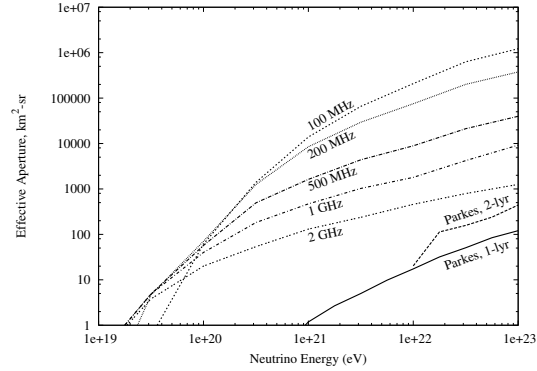


Figure 10: Aperture of the Square Kilometer Array for detection of neutrino interactions in the Moon [116].

radio pulses confirm the theory of Askaryan [112] on which interpretation of measurements in the field will be based. Aspects of propagation of radio signals through the ice-snow-surface interface were checked by observing signals broadcast from a bore hole in the Ross Ice Shelf while ANITA was still in sight [113]. The possibility of using air shower cores to calibrate a radio array in the field was discussed in Ref. [114].

ARIANNA [115] is a proposal to use an array of 10,000 antennas spread over 1000 km<sup>2</sup> just below the snow surface to detect radio signals of neutrinos that interact in the ice. Signals of downward events would be reflected by the ice-water interface.

The history and prospects for using the Moon as the target and large radio telescopes on Earth as the detector is reviewed in Ref. [116]. Figure 10 shows the calculated apertures for various frequencies for the Square Kilometer Array [117]. The apertures for the original measurement with the Parkes telescope [118] are also shown. Techniques for pulse detection and event reconstruction are discussed in Ref. [119]. Although the effective areas achievable can be very large for SKA, as shown in Fig. 10, the energy threshold is well above the range for GZK neutrinos.

**Acoustic detection of neutrinos.** This technique is being explored by measurements in the ice at the South Pole as another approach to achieving the effective volume needed to measure the spectrum of cosmogenic neutrinos [120]. There is also

an acoustic test setup in Lake Baikal [121]. Exploration of acoustic detection in ice is motivated by the lower noise rate in ice as compared to water, which should allow a lower energy threshold for neutrino detection. The goal is to instrument a sufficiently large volume to allow the detection of hundreds of GZK neutrinos per year. The authors suggest a hybrid approach [122] using acoustic, radio and optical detectors to optimize the sensitivity and acceptance of the detector.

**Acknowledgments** This work is supported in part by a grant from the National Science Foundation. I am grateful to Albrecht Karle for helpful comments on the first draft of this paper.

## References

- [1] Kempa, J. & Krawczynska, A., Proc. 30th ICRC, Merida, Mexico (2007) 0989.
- [2] Alvarez, L.W., et al., Science (New Series) 167 (1970) 832.
- [3] Alfaro, R., et al., Proc. 30th ICRC, Merida, Mexico (2007) 1284.
- [4] Adamson, P., et al. (MINOS Collaboration), arXiv:0705.3815.
- [5] Schreiner, P. & Goodman, M. for the (MINOS) Proc. 30th ICRC, Merida, Mexico (2007) 0630.
- [6] Mufson, S. et al. (MINOS), Proc. 30th ICRC, Merida, Mexico (2007) 0709.
- [7] Gaisser, T.K. *Cosmic Rays and Particles Physics* (Cambridge University Press, 1990).
- [8] Zatsepin, G.T. & Kuz'min, V.A., Soviet Physics JETP 12 (1961) 1171.
- [9] deJong, J.K. (MINOS), Proc. 30th ICRC, Merida, Mexico, 2007, 0627.
- [10] Achard, P. et al. (L3 + C) Phys. Lett. B 598 (2004) 15.
- [11] Grashorn, E., et al., (MINOS) Proc. 30th ICRC, Merida, Mexico, (2007) 0697.
- [12] Grashorn, E., et al., (MINOS) Proc. 30th ICRC, Merida, Mexico, (2007) 0696.
- [13] Barrett, P., et al., Revs. Mod. Phys. 24 (1952) 133.
- [14] Ambrosio, M., et al., Astropart. Phys. 7 (1997) 109.
- [15] Bouchta, A., et al., Proc. 26th ICRC, Salt Lake City, Utah (1999) vol. 2, p. 108.
- [16] Barr, G.D., Gaisser, T.K. & Stanev, T.S., 30th ICRC, Merida, Mexico, 2007, 0329.
- [17] Honda, M. et al., 30th ICRC, Merida, Mexico, 2007, 0274.
- [18] Honda, M., et al., Phys. Rev. D 75 (2007) 043006.
- [19] Sanuki, T. et al., Phys. Rev. D 75 (2007) 043005.
- [20] G.D. Barr et al., Phys. Rev. D 70 (2004) 023006.
- [21] M. Honda et al., Phys. Rev. D 70 (2004) 043008.
- [22] Gonzalez-Garcia, M.C., Maltoni, M. & Rojo, J., JHEP 0610 (2006) 075.
- [23] Takahashi, N., et al., Proc. 30th ICRC, Merida, Mexico (2007) 0250.
- [24] Zornoza, J. & Chirkin, D. (IceCube), Proc. 30th ICRC, Merida, Mexico (2007) 0190.
- [25] Lünemann, J. & München, K. (IceCube), 30th ICRC, Merida, Mexico, 2007, 0624.
- [26] Miura, M. (Super-K), Proc. 30th ICRC, Merida, Mexico (2007) 0117.
- [27] Fukuda, Y. et al., Phys. Rev. Letters 81 (1998) 1562.
- [28] Ashie, Y. et al., Phys. Rev. D 71 (2005) 112005.
- [29] Takenaga, Y. (Super-K), Proc. 30th ICRC, Merida, Mexico (2007) 1097.
- [30] Ashie, Y., et al. (Super-K) Phys. Rev. Letters 93 (2004) 101801.
- [31] Higuchi, I. (Super-K), Proc. 30th ICRC, Merida, Mexico (2007) 0818.
- [32] Sousa, A. (MINOS), Proc. 30th ICRC, Merida, Mexico (2007) 0749.
- [33] Michael, D.G. et al. (MINOS) Phys. Rev. Letters 97 (2006) 191801.
- [34] Rebel, B.J. & Mufson, S.L. (MINOS), Proc. 30th ICRC Merida, Mexico (2007) 0711.
- [35] Smy, M. (Super-K) Proc. 30th ICRC, Merida, Mexico (2007) 0213.
- [36] Hirata, K.S. et al., Phys. Rev. Letters 58 (1987) 1490.
- [37] Bionta, R.M. et al., Phys. Rev. Letters 58 (1987) 1494.
- [38] Totani, T., Sato, K. & Yoshii, Y., Ap. J. 460 (1996) 303.
- [39] Kaplinghat, M., Steigman, G. & Walker, T.P., Phys. Rev. D 62 (2000) 043001.
- [40] Beacom, J. & Vagins, M., Phys. Rev. Letters



- 93 (2004) 171101.
- [41] Malek, M. et al., Phys. Rev. Letters 90 (2003) 061101.
- [42] Watanabe, H. et al. (Super-K), Proc. 30th ICRC, Merida, Mexico (2007) 0871.
- [43] Iida, T. et al. (Super-K), Proc. 30th ICRC, Merida, Mexico (2007) 0822.
- [44] Ikeda, M., Takeda, A., et al. (Super-K), Proc. 30th ICRC, Merida, Mexico (2007) 0791.
- [45] Agafonova, N.Y., et al. (LVD), Proc. 30th ICRC, Merida, Mexico (2007) 1022.
- [46] Novoseltsev, Yu., et al. (Baksan), Proc. 30th ICRC, Merida, Mexico (2007) 0442.
- [47] Bahcall, J. & Waxman, E., Phys. Rev. D 64 (2001) 023002 and references therein.
- [48] Hoshina, K., Hodges, J., Hill, G. et al., (IceCube) Proc. 30th ICRC, Merida, Mexico (2007) 1103. See also Achterberg, A., et al. arXiv 0705.1315.
- [49] Tascau, O., Engel, R., Kampert, K-H. & Risse, M., Proc. 30th ICRC, Merida, Mexico (2007) 0183.
- [50] Bugaev, E.v. et al., Phys. Rev. D58 (1998) 054001.
- [51] Gaisser, T.K. & Honda, M., Ann. Revs. Nucl. Part. Sci. 52 (2002) 53.
- [52] Gerhardt, L. et al. (IceCube) Proc. 30th ICRC, Merida, Mexico (2007) 1062.
- [53] Mannheim, K., Protheroe, R.J. & Rachen, J., Phys. Rev. D 63 (2000) 023003.
- [54] Stecker, F., Phys. Rev. D 72 (2005) 107301.
- [55] Mannheim, K., Astropart. Phys. 3 (1995) 295.
- [56] Abdo, A.A. (MILAGRO), Proc. 30th ICRC, Merida, Mexico (2007) 0735.
- [57] Kappes, A., Stegmann, C., Aharonian, F. & Hinton, J., Proc. 30th ICRC, Merida, Mexico (2007) 0777.
- [58] For H.E.S.S. catalog see the following url: <http://www.mpihd.mpg.de/hfm/hess>
- [59] Kappes, A., Hinton, J., Stegmann, C. & Aharonian, F.A., Ap.J. 656 (2007) 870.
- [60] Becker, J.A. et al., Proc. 30th ICRC, Merida, Mexico (2007) 0325.
- [61] Carr, J. et al. (KM3Net), Proc. 30th ICRC, Merida, Mexico (2007) 0865.
- [62] Satalecka, K. Bernardini, E., Ackermann, M., Tluczykont, M. (IceCube), Proc. 30th ICRC, Merida, Mexico (2007) 0582.
- [63] Porrata, R. (IceCube) Proc. 30th ICRC, Merida, Mexico (2007) 0770.
- [64] Aguilar, J.A. (ANTARES), Proc. 30th ICRC, Merida, Mexico (2007) 0638.
- [65] Braun, J., Karle, A., Montaruli, T. (IceCube) Proc. 30th ICRC, Merida, Mexico (2007) 1090.
- [66] Finley, C., Dumm, J., Montaruli, T. (IceCube), Proc. 30th ICRC, Merida, Mexico (2007) 0764.
- [67] Goodman, J., Proc. 30th ICRC, Merida, Mexico (2007) 0622.
- [68] Ackermann, M. et al. (IceCube/AMANDA) and Galante, N. et al. (MAGIC), Proc. 30th ICRC, Merida, Mexico (2007) 1049.
- [69] Kappes, A. et al. (IceCube), Proc. 30th ICRC, Merida, Mexico (2007) 1132.
- [70] Achterberg, A. et al. (IceCube) arXiv:0705.1186 (Ap.J. in press).
- [71] Achterberg, A. et al. (IceCube) Ap.J. 664 (2007) 397.
- [72] Razzaque, S. et al., Phys. Rev. Letters 90 (2003) 241103.
- [73] Murase & Nagatake, Phys. Rev. D73 (2006) 063002.
- [74] Waxman, E. & Bahcall, J., Phys. Rev. Letters 78 (1997) 2292.
- [75] Cronin, J., Hess Lecture, Proc. 30th ICRC, Merida, Mexico (2007).
- [76] Watson, A.A., Plenary talk on Highlights from the Pierre Auger Observatory, Proc. 30th ICRC, Merida, Mexico (2007).
- [77] Teshima, M. Rapporteur talk on extensive air showers and UHE cosmic rays, Proc. 30th ICRC, Merida, Mexico (2007).
- [78] Greisen, K., Phys. Rev. Letters 16 (1966) 748.
- [79] Zatsepin, G.T. & Kuz'min, V.A., Pisma Zh. Experim. Theor. Phys. 4 (1966) 114.
- [80] Blanch-Bigas, O. (Auger) Proc. 30th ICRC, Merida, Mexico (2007) 0603.
- [81] Martens, K., (HiRes), Proc. 30th ICRC, Merida, Mexico (2007) 1194.
- [82] Ackermann M., et al., Astropart. Phys. 22 (2005) 339.
- [83] Aynutdinov, V. et al., Astropart. Phys. 25 (2006) 140.
- [84] Kravchenko, I. et al., Phys. Rev. D 73 (2006) 082002.

- [85] Barwick, S.W. et al., Phys. Rev. Letters 96 (2006) 171101.
- [86] Lehtinen, N.G. et al., Phys. Rev. D 69 (2004) 013008.
- [87] Gorham, P.W. et al., Phys. Rev. Letters 93 (2004) 041101.
- [88] Engel, R., Seckel, D. & Stanev, T., Phys. Rev. D64 (2001) 093010.
- [89] Allard, D. et al., JCAP 9 (2006) 5.
- [90] Busca, N.G. et al., Proc. 30th ICRC, Merida, Mexico (2007) 0852.
- [91] Kouchner, A. (Antares), Proc. 30th ICRC, Merida, Mexico (2007) 0089.
- [92] Karle, A. (IceCube) Proc. 30th ICRC, Merida, Mexico (2007) 1180.
- [93] Pretz, J. et al. (IceCube) Proc. 30th ICRC, Merida, Mexico (2007) 1018.
- [94] Gaisser, T. et al. (IceCube) Proc. 30th ICRC, Merida, Mexico (2007) 0758.
- [95] Gross, A. et al., (IceCube) Proc. 30th ICRC, Merida, Mexico (2007) 1013.
- [96] Grullon, S. et al. (IceCube) Proc. 30th ICRC, Merida, Mexico (2007) 1107.
- [97] Taiuti, M. (NEMO) Proc. 30th ICRC, Merida, Mexico (2007) 0856.
- [98] Anassontzis, E.G. et al. (NESTOR), Nucl. Phys. Proc. Suppl. 85 (2000) 50.
- [99] Carr, J. et al. (KM3Net) Proc. 30th ICRC, Merida, Mexico (2007) 0859.
- [100] White, R.J. (KM3Net) Proc. 30th ICRC, Merida, Mexico (2007) 1067.
- [101] Zas, E. New Journal of Physics, 7 (2005) 130.
- [102] Borriello, E., et al., Proc. 30th ICRC, Merida, Mexico (2007) 0004.
- [103] Cuoco, A., et al., JCAP 0702:007 (2007).
- [104] Góra, D., Roth, M. & Tamburro, A., Proc. 30th ICRC, Merida, Mexico (2007) 0160.
- [105] Alvarez-Muniz, J., James, C.W., Protheroe, R.J. & Zas, E., Proc. 30th ICRC, Merida, Mexico (2007) 0459.
- [106] Provorov, A.L. & Zheleznykh, I.M., Astropart. Phys. 4 (1995) 55.
- [107] Zheleznykh, I.M. et al., Proc. 30th ICRC Merida, Mexico (2007) 1139.
- [108] Kravchenko, I. (RICE), Proc. 30th ICRC, Merida, Mexico (2007) 0659.
- [109] Landsman, H., L. Ruckman, G.S. Varner, Proc. 30th ICRC, Merida, Mexico (2007) 1155.
- [110] Palladino, K.J. (ANITA) Proc. 30th ICRC, Merida, Mexico (2007) 1095.
- [111] Kowalski, J. (ANITA) Proc. 30th ICRC, Merida, Mexico (2007) 0929 and Gorham, P.W., Phys. Rev. Letters (hep-ex/0611008).
- [112] Askaryan, G.A., JETP 21 (1965) 658.
- [113] Goldstein, D., Hoover, S., Nam, J. (ANITA) Proc. 30th ICRC, Merida, Mexico (2007) 1219.
- [114] Seckel, D., Proc. 30th ICRC, Merida, Mexico (2007) 0806.
- [115] Barwick, S.W. (ARIANNA), Proc. 30th ICRC, Merida, Mexico (2007) 1163.
- [116] James, C.W., Ekers, R.D., McFadden, R. & Protheroe, R.J., Proc. 30th ICRC, Merida, Mexico (2007) 0431.
- [117] Terzian, Y. & Lazio, J. in *Ground-based and Airborne Telescopes* (ed. L.M. Stepp), Proc. SPIE (2006) 6267.
- [118] Hankins, T.H., Ekers, R.D. & O'Sullivan, J.D., Monthly Not. Roy. Astron. Soc. 283 (1996) 1027.
- [119] McFadden, R.A. et al., Proc. 30th ICRC, Merida, Mexico (2007) 0434.
- [120] Böser, S. et al. (SPATS) Proc. 30th ICRC, Merida, Mexico (2007) 1142 and 1282.
- [121] V. Prosin & R. Wischniewski (Baikal) Proc. 30th ICRC, Merida, Mexico (2007) 0639.
- [122] Besson, D. et al., Int. J. Mod. Phys. A21S1 (2006) 259.